
Modality Collapse as Mismatched Decoding: Information-Theoretic Limits of Multimodal LLMs

Jayadev Billa*
jbilla2004@gmail.com

Abstract

Numerous studies have shown that multimodal LLMs process speech and images well but fail in non-intuitive ways rendering trivial tasks such as object counting unreliable. We investigate this behavior from an information-theoretic perspective by framing multimodal LLM inference as a *mismatched decoder* problem: a decoder trained primarily on text can only extract information along text-aligned directions (removing up to 98% of the variation in modality-specific (non-text) directions *improves* decoder loss) and the amount of accessible information is bounded by the Generalized Mutual Information (GMI). We show that information loss is bounded as the distributional mismatch between the source data and the text data increases, and as the sensitivity of the decoder increases. This bound is a function of the model’s scoring rule not its architecture. We validate the predictions across five models spanning speech and vision. A controlled study (two Prismatic VLMs differing only in encoder text-alignment) shows that the bottleneck lies in the scoring rule of the decoder rather than the text-alignment of the encoder or the learned projection. A LoRA intervention demonstrates that simply training with an emotion-related objective improves emotion detection from 17.3% to 61.8% task accuracy without affecting other attributes, confirming that the training objective determines what becomes accessible.

https://github.com/jb1999/modality_collapse_paper

1 Introduction

Multimodal LLMs follow a common recipe: an encoder processes the non-text input (speech, image), a learned projection maps it into the LLM’s embedding space, and the LLM generates a text response (Liu et al., 2023; Dai et al., 2023; Fixie AI, 2024; Chu et al., 2024; Karamcheti et al., 2024). These systems appear to perform well on standard benchmarks. However, there are many reported gaps in model performance (Chen et al., 2026; Cuervo et al., 2026; Thrush et al., 2022; Yüksekönül et al., 2023; Jain et al., 2025) where even some trivial tasks are not resolved. A model might produce a perfect response to speech input but have no understanding of the emotional state of the speaker; it may correctly identify every object in an image and yet fail to count the number of objects or understand the spatial relationships. Here, the information is clearly available to the model, since it can list every object, but it cannot make use of this available information for all tasks. We refer to this selective failure as *modality collapse*.

To provide insight into this behavior we borrow the well-defined concept of a *mismatched decoder* from communication theory, where a decoder originally designed for source A receives source B. A multimodal LLM fits this definition of a mismatched decoder exactly: an LLM trained to “decode” text representation is now expected to extract information from audio and/or image projections. Our mismatched decoder analysis is a formalization of the perception constraint cost (Blau & Michaeli, 2019).

In this framing the accessible information is bounded by the Generalized Mutual Information (GMI) not standard mutual information, as would be the case for matched decoders. We

*Unaffiliated researcher; previously at ISI@USC, Yahoo, Nuance, and BBN.

refer to this difference as the *information accessibility gap*. The gap is not about architecture; it is about the scoring rule. No explicit adapter module is required: any system where a text-trained decoder processes non-text representations faces the same constraint, whether the representations arrive through a learned projection, a discrete codebook, or the LLM’s own layers. At inference, every trained model has fixed weights: the scoring rule is whatever the training procedure produced. A model trained predominantly on text has a text-shaped scoring rule regardless of whether the LLM was frozen or fine-tuned during training. What matters is the training objective, not which components were updated (§6.1).

What causes this gap? A transformer model is sensitive to its input in all directions; one trained on text is still sensitive to non-text directions (we validate this empirically using gradient isotropy in §5.6). That said, its sensitivity to non-text directions is unproductive. The decoder treats unfamiliar structure as noise, and noise hurts its text processing, as would be expected in a *mismatched decoder*. In §5.4 we empirically show that removing up to 98% of the variation in modality-specific (non-text) directions *improves* decoder loss; the decoder is not indifferent to non-text directions, but responds to them in destructive ways. We can quantify this degradation (Theorem 2). It is proportional to both the distributional distance between the modality and text representations and the decoder’s sensitivity to this distance (its Lipschitz constant L_{\log} , which measures how much the output changes per unit change in the input). This sensitivity can be up to $30\times$ that of a linear probe (a classifier trained on frozen representations to test what information is present; Theorem 3, §A.5). Text-aligned encoders reduce the distance (§5.5), but only by discarding non-textual information earlier on. The collapse occurs earlier, not less.

Contributions. (1) We formalize modality collapse as mismatched decoding, and prove that the accessible information is at most the GMI, and degrades with the distributional mismatch and the sensitivity of the decoder (§4). (2) On five models and two modalities, we show that the information accessibility gap is present: non-text information is preserved by the LLM but is not decodable because the decoder is not incentivized to use it (§5.4, §5.2). (3) We run a controlled study on Prismatic VLMs (identical architecture, identical LLM, only text-alignment of the encoder changes), and show that the scoring rule is the causal factor (§5.5). (4) We run a LoRA intervention that confirms the prescription: training with an emotion objective improves emotion task accuracy from 17.3% to 61.8% (+7.5% probe), while training with a text objective does not (§6.1).

2 Related work

Multimodal LLMs and the adapter paradigm. The practice of projecting encoded representations into the embedding space of an LLM has been widely adopted for both vision (Liu et al., 2023; Dai et al., 2023; Zhu et al., 2024; Karamcheti et al., 2024; Tong et al., 2024) and speech (Fixie AI, 2024; Chu et al., 2024). While these approaches perform well on text-centric tasks, they perform poorly on tasks that require modality-specific knowledge, a phenomenon observed empirically but not understood theoretically.

Modality gap. Liang et al. (2022) observed that the CLIP embeddings of different modalities are separated by a “modality gap” in the shared space. More recently, Huh et al. (2024) reported that the representations of different modalities become similar. While our results are largely orthogonal to these geometric findings, we provide an information-theoretic explanation for the modality gap: it is not that information is lost, but rather that the decoder is unable to make use of information in unfamiliar directions.

Modality collapse. Javaloy et al. (2022) use this term to describe models that discard an entire modality during training due to gradient conflicts. Our usage describes a subtler failure: the model processes all modalities and preserves their information internally, but the decoder selectively fails to use non-primary-modality content.

Mismatched decoding. The mismatched decoder framework (Merhav et al., 1994; Lapidath, 1996; Scarlett et al., 2020) provides the data rates supported by a decoder mismatched to its incoming channel. We borrow this approach and apply it to the multimodal LLM framework. At inference time, any LLM that uses a scoring rule that was learned via a

text-dominant training procedure is a mismatched decoder when applied to non-text inputs. The mismatch arises from the loss function, not from what parameters were updated.

Representation probing. Linear probes are a common method for probing the information content of neural representations (Alain & Bengio, 2017; Conneau et al., 2018; Hewitt & Manning, 2019; Belinkov, 2022). We do not use probing to argue that some information is “encoded” in a representation, but to highlight the difference between information that is *present* (probe-recoverable) and information that is *accessible* (decoder-extractable).

Rate-distortion-perception (RDP) in ML. Blau & Michaeli (2019) formalized perceptual quality as a distributional constraint: reconstructions are perceptually good when their distribution matches the real data distribution. The text-trained decoder imposes a perception constraint (text-aligned directions), forcing the adapter to compromise modality-specific information to satisfy the constraint. We draw on this framework in §3, where the decoder takes the role of the perceptual evaluator.

3 Problem formulation

Architecture. We consider the typical multimodal LLM pipeline:

$$X \xrightarrow{E} H \xrightarrow{A} Z \xrightarrow{L(\cdot, C)} \hat{Y} \quad (1)$$

where X is a non-text input (speech waveform or image), E is a pre-trained encoder (e.g., Whisper (Radford et al., 2023), CLIP (Radford et al., 2021)), A is a learned adapter, $Z \in \mathbb{R}^d$ are the hidden states consumed by the LLM L , C is the text context (prompt), and \hat{Y} is the generated output. The specific form of A varies (linear, MLP, Q-Former (Dai et al., 2023), perceiver, codebook), but the mismatch depends on the scoring rule, not the adapter type (§6.1).

Scoring rule, text law and modal law. Let $q(y|z, c)$ denote the LLM’s next-token distribution at inference. This is the fixed scoring rule resulting from training. During pre-training, the LLM processes hidden states drawn from the text law $P_T(C, Z, Y)$. When processing adapted non-text inputs, the hidden states follow a different modal law $P_M(C, Z, Y)$.

We assume the text and modal laws share the same prompts and target tokens ($P_M(C, Y) = P_T(C, Y)$), so the only difference is in the representations Z . The quantitative bound (§4) additionally requires that the decoder’s log-score is Lipschitz continuous and that representations occupy a bounded region (Assumptions 2, 3 in Appendix A.2, validated empirically in §5.6).

Formalizing modality collapse. The earlier intuitive explanation of modality collapse (information is available but the decoder cannot use it) can be stated precisely. For an attribute S_τ of type τ (e.g., speaker identity, emotion), we define the *information accessibility gap* as:

$$\Delta_{\text{access}}(\tau) = I(Z; S_\tau) - \text{GMI}_{P_M}(S_\tau | q) \quad (2)$$

where $I(Z; S_\tau)$ is the information about S_τ present in the representation and $\text{GMI}_{P_M}(S_\tau | q)$ is the information actually extractable by the decoder’s fixed scoring rule. When $\Delta_{\text{access}} = 0$, the decoder extracts everything present; when Δ_{access} is large, information is present but inaccessible.

Implicit RDP tradeoff. Blau & Michaeli (2019) formalized perceptual quality as a distributional constraint: reconstructions are perceptually good when their distribution matches the real data distribution, measured as a divergence $d(p_X, p_{\hat{X}})$. In our setting, the perceptual evaluator is the decoder itself. A text-trained decoder implicitly judges representations by how closely they resemble its training distribution P_T ; representations drawn from a different distribution P_M are treated as low quality regardless of their information content. When $P_M \neq P_T$, the adapter must sacrifice modality-specific content (distortion) to produce representations the decoder can process. We measure this perception cost using the Wasserstein distance $W_1(P_M, P_T)$, chosen because it aligns with the Lipschitz continuity of the decoder to yield the GMI bound (§4); other divergences would capture the same

mismatch but without this property. The role of adapter capacity (the rate dimension of the tradeoff) is a direction for future work.

Text-aligned encoders as correlation mappings. Contrastive encoders like CLIP (Radford et al., 2021) and SigLIP (Zhai et al., 2023) do not merge the modality manifolds (the modality gap persists (Liang et al., 2022)), but they align the *informative directions*: attributes that co-occur with text descriptions occupy dimensions also used by text representations. When such an encoder feeds an LLM, the modal law P_M has high overlap with P_T along informative dimensions, so the distributional distance is small and the accessibility gap is correspondingly small (we formalize this in terms of the Wasserstein distance in §A.2). Non-contrastive encoders like DINOv2 (Oquab et al., 2024) lack this alignment: their informative directions may be orthogonal to P_T , making the information effectively inaccessible to the decoder. We return to this in §5.5, where the Prismatic comparison provides direct evidence.

4 Theoretical framework

The mismatched decoder framing makes three concrete predictions. First, since the decoder was trained on text, there should be an upper limit on how much non-text information it can extract, regardless of how much is present in the representation. Second, this limit should get worse as the modality representations diverge from text. Third, a simple classifier (a linear probe) trained directly on the representations should not be subject to the same limit, since it is not constrained by a text-trained scoring rule. We formalize each below (formal statements, assumptions, and proofs in Appendix A):

1. The decoder has an upper bound. The standard mutual information $I(Z; Y)$ represents the information Z contains about Y assuming an optimal decoder. But the LLM is not an optimal decoder for non-text inputs, given a text-focused training objective. Instead, the relevant quantity is the Generalized Mutual Information (GMI) (Merhav et al., 1994; Scarlett et al., 2020), the maximum rate achievable with a fixed scoring rule. No matter how much information any probe can get from Z , the decoder is always bounded by $\text{GMI}_{P_M}(q)$ (Theorem 1).

2. The ceiling drops with distributional distance. The GMI decreases when the modal representations P_M differ from the text representations P_T the decoder was trained on. How much it drops depends on two measurable quantities: how far the modal representations are from text (the Wasserstein distance W_1), and how sensitive the decoder is to that difference (the Lipschitz constant L_{\log}). The drop is bounded by their product (Theorem 2). Both quantities can be estimated from a trained model (W_1 from the representations, L_{\log} from gradient norms), so the bound yields a testable prediction: models with larger $L_{\log} \cdot W_1$ should show more degradation. We validate this ranking in §5.6. In the high-mismatch regime the bound is numerically loose, but it remains an ordinal diagnostic: it correctly ranks model–modality pairs by collapse severity and predicts which information types degrade (Appendix A.3 tightens the prefactor from $\sim e^{150}$ to $\sim e^7$).

3. Probes and decoders respond differently to the same shift. For a linear probe, the effect of a distributional shift is bounded by the (small) Lipschitz constant L_h (Theorem 3). For the decoder, it is bounded by L_{\log} , which is empirically $30\times$ larger. A W_1 shift of the same magnitude therefore results in a small degradation for probes and a large degradation for the decoder. This is the formal basis for the accessibility gap: the same information can be simultaneously recoverable by a probe and unusable by the decoder, because the two have vastly different sensitivity to distributional mismatch.

The three propositions above establish the perception-distortion face of the RDP tradeoff: as the distributional distance $W_1(P_M, P_T)$ grows, accessible information (GMI) decreases, and the decoder is disproportionately more affected than a probe.

Model	Encoder	Text-aligned?	LLM
Ultravox	Whisper	No	Llama-3.1-8B
Qwen2-Audio	Whisper	No	Qwen2-7B
LLaVA	CLIP-ViT	Yes	Vicuna-7B
Prismatic-D	DINOv2	No	Vicuna-7B
Prismatic-S	SigLIP	Yes	Vicuna-7B

Table 1: Models studied. Prismatic-D and Prismatic-S share the same architecture, adapter, training recipe, and LLM backbone; only the vision encoder differs.

5 Experimental validation

5.1 Setup

Models. We investigate five multimodal LLMs across two modalities (Table 1). For speech: **Ultravox-v0.6** (Fixie AI, 2024) (Whisper encoder, MLP adapter with SwiGLU, Llama-3.1-8B) and **Qwen2-Audio-7B** (Chu et al., 2024) (Whisper encoder, linear adapter, Qwen2-7B). For vision: **LLaVA-v1.5-7B** (Liu et al., 2023) (CLIP-ViT, MLP adapter, Vicuna-7B) and two **Prismatic VLMs** (Karamcheti et al., 2024) with the same MLP adapter and Vicuna-7B backbone but with different vision encoders: **DINOv2** (not text-aligned) and **SigLIP** (text-aligned via contrastive loss).

Datasets. Speech: LibriSpeech (Panayotov et al., 2015) (2,620 samples, 50 words, 40 speakers), CREMA-D (Cao et al., 2014) (7,442 samples, 6 emotions, 91 speakers), ESC-50 (Piczak, 2015) (2,000 samples, 50 sound classes). Vision: MS-COCO (Lin et al., 2014) (5,000 images, 69 object categories, 12 super-categories).

Probing protocol. We consider four hook points per model: encoder output, adapter output, LLM layer 16, and LLM final layer (after LayerNorm). Representations are mean-pooled across sequence positions. Ultravox also provides audio token boundaries, but pooling over audio-only tokens results in nearly identical trends (see Appendix Table 9). For each hook point, information type and dataset combination, we train ℓ_2 -regularized logistic regression probes (5 seeds, 80/20 stratified split, z-score normalization).

Information types. Speech: *lexical* (word identity), *speaker* (speaker identity), *emotion* (6-way), *acoustic* (sound class). Vision: *lexical* (caption-based word prediction), *object category* (69-way), *super-category* (12-way).

The Prismatic pair (shared architecture, different encoder) and the two speech models (shared encoder, different LLM) serve as controls that allow us to isolate these specific variables.

5.2 The information accessibility gap in practice

Linear probes across layers show that for all 5 models, non-text information is not destroyed by the LLM (Appendix Tables 5 and 7): at the final layer, speaker identity is $22\times$ above chance for Ultravox and object categories are $55\times$ above chance in Prismatic-D (.792 vs. .014). The information is preserved. Does the decoder use it?

The answer depends on text-alignment. In both speech models, the LLM approximately doubles lexical information (+92% Ultravox, +95% Qwen2-Audio), but degrades speaker identity (−8% to −39%). When the encoder is text-aligned (CLIP in LLaVA, SigLIP in Prismatic-S), $P_M \approx P_T$ and all information types improve (+5–8%). The decoder amplifies what it was trained on and is indifferent to the rest. The LISTEN benchmark (Chen et al., 2026) independently observed this pattern: audio LLMs predict emotions based on what the speaker *says* rather than *how* they say it. Our framework explains why: the text-shaped scoring rule amplifies lexical content (+92–95%) while remaining indifferent to acoustic features, so emotion predictions are driven by word choice rather than prosody.

The same pattern appears in vision, though in a weaker mismatch regime (Appendix Table 10). Three visual features not present in text (object count, object size, spatial distribution) show flat or modest improvement through the LLM ($L_{\log} \cdot W_1 \approx 13\text{--}54$ vs. 162 for speech), consistent with stagnation unlike the sharp degradation in speech.

5.3 Mode alignment

The bound describes how much information is lost; mode alignment tells us the directions in which it is lost. We perform a principal component analysis of the adapter’s output representations under the modal distribution, yielding a covariance matrix Σ_M with eigenvectors u_k and eigenvalues λ_k , sorted by decreasing eigenvalue. We refer to each eigenvector as a *mode*: Mode 0 is the direction along which the adapter’s output varies the most, Mode 1 the next, and so on. For each mode, we ask: has the decoder seen variation along this direction during training? The alignment score

$$\rho_k = u_k^\top \Sigma_T u_k / \lambda_k$$

is the Rayleigh quotient of the text covariance Σ_T evaluated along the modal eigenvector u_k , normalized by the modal eigenvalue λ_k . The numerator measures how much the text distribution varies along direction u_k ; the denominator is how much the modality varies along the same direction. When $\rho_k = 1$, the text and modal distributions have equal variance along u_k , so the decoder has been trained on exactly this kind of variation and can use it. When $\rho_k \approx 0$, the modality varies along a direction where text has almost no variance: the decoder has never seen input spread along this direction and cannot productively respond to it. We label modes with $\rho_k < 0.5$ as modality-specific (MS); the threshold is a practical cutoff, and results are not sensitive to the exact value (Appendix Table 11).

For non-aligned speech encoders, Mode 0 (the direction of largest adapter variance) is modality-specific ($\rho_0 \leq 0.034$), accounting for 51–79% of adapter variance. For Prismatic-DINOv2, Mode 0 is also modality-specific ($\rho_0 = 0.034$) but carries only 8% of variance; the MS variance is instead distributed across 53 modes (71% total; Table 11). In both cases, the dominant source of variation in the adapter’s output is invisible to the text distribution. For SigLIP, even Mode 0 is text-aligned ($\rho_0 = 0.83$): the encoder has already organized its output along text-like directions. As representations pass through the LLM, text-aligned variance is amplified ($\sim 150\times$) while MS variance is unaffected: MS modes go from 63.6% of adapter variance to $< 1\%$ at the final layer in Ultravox, not destroyed but drowned out.

5.4 Modality-specific structure interferes with decoding

Probes show that non-text information is present; causal ablation tests whether the decoder is impacted by it. Unlike concept erasure methods such as LEACE (Belrose et al., 2023), which eliminate directions predictive of a labeled attribute, we ablate directions identified by distributional mismatch without concept labels. For each mode classified as MS ($\rho_k < 0.5$) in §5.3, we remove its contribution from the representation: $z' = z - \sum_{k \in S} (z^\top u_k) u_k$, and compare three conditions (200 samples per model): (i) ablate all MS modes, (ii) ablate a matched number of top TA modes, (iii) no ablation.

MS structure is not merely unused; its presence degrades decoding. Removing variance from a representation should hurt performance since there is strictly less information available. Yet for non-aligned encoders, removing MS modes improves decoder loss (Table 2). Qwen2-Audio provides the cleanest demonstration: 5 MS modes carry 97.6% of adapter variance, yet removing them improves loss (-0.1% , $t = -9.0$), while removing 5 TA modes (only 1.8% of variance) hurts $7\times$ more ($+1.0\%$, $t = 27.8$). Nearly all of the adapter’s variance is dispensable; a tiny fraction carrying text-aligned information is essential. Prismatic-D confirms the pattern at larger scale: ablating 53 MS modes (71% of adapter variance) decreases cross-entropy by 11.1% ($t = -25.2$), while ablating a matched number of TA modes has no detectable effect (-0.07% , $t = -0.4$, $p = 0.69$). For Ultravox the effect is smaller (-1.4%) but still significant ($t = -7.0$). The decoder is not just indifferent to MS directions, it is actively harmed by them.

Model	Condition	Modes	Var. %	Δ Loss (%)
<i>Non-aligned encoders</i>				
Ultravox	MS (all)	11	63.6	-1.4
	TA-matched	11	29.4	-0.3
	Random	11	2.8	+0.3
Qwen2-Audio	MS (all)	5	97.6	-0.1
	TA-matched	5	1.8	+1.0
	Random	5	0.1	+0.2
Prismatic-D	MS (all)	53	71.0	-11.1
	TA-matched	47	29.0	-0.07
	Random	53	39.1	-5.1
<i>Text-aligned encoder</i>				
Prismatic-S	MS (all)	14	24.6	-0.5
	TA-matched	14	36.2	-0.7
	Random	14	10.6	-0.2

Table 2: Causal ablation at the adapter output. Eigenmodes are classified as modality-specific (MS; $\rho_k < 0.5$) or text-aligned (TA), and matched subsets are projected out. Random controls ablate the same number of modes chosen uniformly at random (seed-averaged). For non-aligned encoders, removing MS modes improves loss while removing equal-sized TA subsets has negligible effect; the contrast is $160\times$ for Prismatic-D ($t = -25.2$ vs. $t = -0.4$). Random ablation gives intermediate effects proportional to variance removed. For SigLIP, few modes are MS and all effects are $< 1\%$.

For Prismatic-S (text-aligned), only 14 of 100 modes are MS (24.6% of variance) and all ablation effects are below 1%, consistent with SigLIP representations already matching what the decoder expects.

5.5 Controlled experiment: text-aligned vs. non-aligned encoders

The causal ablation shows that MS directions influence decoding. Now, we explain *why* some models have more MS variability than others. The Prismatic pair is ideal for this, as it controls for all factors except the text-alignment of the encoder.

Both Prismatic VLMs use the same MLP adapter, Vicuna-7B backbone architecture and training protocol. The difference lies in the vision encoder: DINOv2 (Oquab et al., 2024) (no text alignment) versus SigLIP (Zhai et al., 2023) (contrastive text-image loss). According to our hypothesis, the representations learned by SigLIP should be more similar to P_T , leading to smaller $W_1(P_M, P_T)$ and less information loss.

This is what we see (Appendix Table 10): the split is sharper for non-textual attributes (object count, object size, spatial spread), which cannot be inferred from captions alone. For these features, SigLIP shows consistent improvement through the LLM (+4.5–8.2%) while DINOv2 gains less (+1.3–4.7%), with the largest gap on object count (+8.2% vs. +3.4%).

For DINOv2, visual information (object category, super-category) passes through the LLM unchanged ($\pm 0.4\%$), neither amplified nor degraded. For SigLIP, the same information is amplified (+1.9% object category, +2.3% super-category). The contrast confirms the prediction: a text-aligned encoder produces representations the decoder can productively process; a non-aligned encoder produces representations the decoder is indifferent to. For LLaVA (CLIP encoder, text-aligned), all information types improve (Appendix Table 7). The effect sizes in vision are modest ($\pm 2\%$) compared to speech ($\pm 39\%$), consistent with the lower mismatch regime ($L_{\log} \cdot W_1$ is 3–12 \times smaller for vision). The value of the Prismatic comparison lies not in the magnitude but in the isolation of the causal variable: same architecture, same adapter, same LLM, same training with the only difference being the encoder’s text-alignment.

5.6 Validating the bound

L_{\log} is finite for all nine model-dataset pairs, validating the Lipschitz assumption (Appendix Table 8). It varies with content (9.08 for speech to 3.66 for environmental sounds in Ultravox) and differs $30\times$ across architectures (0.29 LLaVA to 9.08 Ultravox). Prismatic-S has $2.8\times$ larger L_{\log} than Prismatic-D (1.12 vs. 0.40): the decoder is more responsive to representations that resemble text.

Gradient isotropy. To check whether the decoder selectively ignores MS directions at the gradient level, we compute the norm of the decoder’s loss gradient when the input representation is perturbed along each eigenmode direction. Let $g_k = |\nabla_{u_k} \mathcal{L}|$ be the gradient norm for mode k . The mean gradient norm for TA modes (\bar{g}_{TA}) and MS modes (\bar{g}_{MS}) are nearly equal ($\bar{g}_{\text{TA}}/\bar{g}_{\text{MS}} = 0.94$, Spearman $r = 0.11$, $p = 0.28$): the decoder does not selectively ignore MS directions. This confirms the scalar L_{\log} assumption.

The product $L_{\log} \cdot W_1$ ranks models by collapse severity. Ultravox ($L_{\log} \cdot W_1 = 162$) shows the most degradation (-39% speaker); LLaVA (13.4) shows none. Prismatic-S has a higher product (53.7) than Prismatic-D (20.2) despite less degradation, reflecting greater decoder responsiveness to text-aligned representations rather than greater mismatch. As noted in §4, the bound is an ordinal diagnostic: it correctly ranks models and predicts which information types degrade, even in the high-mismatch regime where it is numerically loose (Appendix A.3, A.4).

6 Discussion

6.1 Implications

The fix is objective-side, not encoder-side. If modality collapse is a result of the scoring rule being text-shaped, a logical solution would be to reshape the scoring rule. Low-rank adaptation (LoRA; Hu et al., 2022) on the LLM modifies q to make it closer to P_M , effectively reducing the functional mismatch. Preliminary evidence from concurrent work on audio-text conflict supports this: applying LoRA to the LLM backbone decreases text dominance, whereas adapter-only training *increases* it.¹ This is predicted by Theorem 2: LoRA reduces the functional mismatch between P_M and P_T by reshaping the scoring rule, whereas adapter-only training does not change the decoder’s text-shaped sensitivity.

However, LoRA on the decoder is *necessary but not sufficient*: the training objective must explicitly target non-text information. We show this with a LoRA experiment on Ultravox ($r=16$, $\alpha=32$, targeting q/k/v/o.proj).

LoRA with emotion objective. We fine-tune with LoRA on the LLM backbone using a forced-choice emotion detection objective on CREMA-D (6 emotions, 7,442 clips, standard causal LM loss on assistant tokens only). We evaluate the effect of LoRA on two measures: linear probe accuracy at the LLM’s final layer (measuring what information is accessible in the representation) and task accuracy (measuring whether the decoder actually uses it in its output). Task accuracy on held-out samples improves from 17.3% to 61.8% (Table 3). The *emotion probe* at llm-final improves from $.557 \pm .006$ to $.632 \pm .011$ (+7.5%), while the speaker probe remains at chance ($.135 \pm .006$ vs. $.137 \pm .008$) and lexical accuracy stays near-ceiling ($.994 \pm .001$). Upstream layers (encoder, adapter) are shared between conditions, so this is purely a change to the LLM. LoRA modifies the scoring rule such that at inference, the decoder will respond to the subset of directions that are emotion-relevant and leave the rest unchanged. Consistent with Theorem 2, the emotion objective reduces W_1 along the subset of directions correlated with emotion, while leaving all others unchanged.

Text-aligned encoders are a workaround, not a solution. Contrastive encoders like CLIP and SigLIP achieve low mismatch because they project the input data into the space of text-correlated features. The alignment is effective but selective in that it preserves what co-occurs with text and discards the rest. The Prismatic comparison shows that SigLIP’s

¹Citation omitted for double-blind review.

Table 3: LoRA intervention on Ultravox (CREMA-D, llm-final probe accuracy). The emotion LoRA selectively improves emotion accessibility without meaningfully affecting speaker or lexical probes. Task accuracy measures forced-choice emotion detection on 1,002 held-out samples. The encoder and adapter outputs are identical across conditions (LoRA modifies only the LLM).

Condition	Emotion (probe)	Speaker (probe)	Lexical (probe)	Task acc.
Base Ultravox	.557	.137	.999	17.3%
+ Emotion LoRA	.632	.135	.994	61.8%
Δ	+7.5%	-0.2%	-0.5%	+44.5%

visual representations “enhanced” by the LLM in fact only looked better because they were pre-projected into text-like directions. CLIP provides the LLM with visual features organized along text-correlated dimensions; genuinely visual information (texture, spatial layout) is discarded upstream.

Models must be explicitly trained to use non-text modalities. A text-only decoder will not listen to signals it was not trained on (§5.3). No adapter can make it sensitive to directions it has never seen. If we want a model to use modality-specific knowledge, rather than merely its text representation, we need to provide a training signal for it to do so, whether through LoRA, full multimodal pretraining, or some other objective-side intervention such as a modality-specific loss. Otherwise the information is just not available.

The framework is architecture-agnostic. The bound we present depends on the decoder’s scoring rule not the model’s architecture. The source of representations, a linear projection, an MLP, a Q-Former, a discrete codebook (Borsos et al., 2023; Défossez et al., 2024), or no explicit adapter at all (i.e., the LLM’s own layers act as the adapter), is immaterial. Discrete token methods introduce an additional quantization bottleneck that can only increase $W_1(P_M, P_T)$, making our bound more conservative. The essential phenomenon is the distributional shift the decoder sees between training and inference.

6.2 Limitations

Probes as information measures. Linear probes provide a necessary but not sufficient condition for information presence (Belinkov, 2022), but the main asymmetry (more information can be linearly recovered than the decoder uses) holds either way. We can only approximate L_{\log} via p95 gradient norms, not compute the true supremum. Other caveats (in scope, Assumption 1) can be found in Appendix C.

Vision collapse is partial. In vision models, we observe a plateau in performance ($\pm 1-2\%$) rather than a drop (-39% for speech). This is consistent with the bound: in a low $L_{\log} \cdot W_1$ regime ($3-12\times$ smaller than speech), the GMI ceiling is close to the matched-decoder rate, so collapse manifests as stagnation rather than degradation. The causal ablation confirms that MS structure still interferes even when probe accuracy is unchanged (Prismatic-D: -11.1% , $t = -25.2$). Probing purely visual features (texture, depth, material) rather than text-describable categories would likely reveal stronger collapse.

Scale. All five models studied are in the 7–8B parameter range. The bound (Theorem 2) depends on the scoring rule’s sensitivity (L_{\log}) and the distributional distance (W_1), not on parameter count, so the theoretical constraint is scale-invariant. For larger models the bound should remain consistent with our results insofar as a text-majority-training-objective paradigm remains. Validating the bound at the 70B scale is a direction for future work.

7 Conclusion

Modality collapse is caused by a failure of *decoding*, not encoding, as our experiments demonstrate. The GMI-Wasserstein bound shows theoretically that only information in the

text-aligned directions is accessible to the decoder, and the rate at which information is lost depends on distributional divergence and decoder sensitivity.

To train multimodal models that properly exploit the information they receive, it is necessary to adjust the scoring function of the decoder. Text-aligned encoders do appear to improve performance, but they do so by ignoring all non-text modalities at the level of the encoder. Our LoRA experiment confirms this: an emotion-based objective trains the decoder to be sensitive to emotion-relevant messages (+7.5% probe, +44.5% task accuracy), without affecting irrelevant messages. The question, for any multimodal model, is not whether modality-specific details can be represented (they are) but whether the training objective instructs the decoder to rely on them.

Reproducibility statement

All models are publicly available. Complete reproduction code, pipeline scripts, and expected-value regression tests are available at https://github.com/jb1999/modality_collapse_paper. Hook points, hyperparameters, and seeds are in Appendix B. All experiments run on a single NVIDIA RTX 3090 Ti (24GB).

Ethics & AI disclosure

This work analyses existing publicly available models and datasets; no new data was collected and no human subjects were involved. The author used Claude/Claude Code during preparation for manuscript critique, narrative feedback, literature search, and experiment implementation and debugging. All research design, theoretical development, experimental execution, analysis, and writing are the author’s own. The author takes full responsibility for all content.

References

- Guillaume Alain and Yoshua Bengio. Understanding intermediate layers using linear classifier probes. In *Proceedings of the 5th International Conference on Learning Representations (ICLR), Workshop Track*, 2017.
- Yonatan Belinkov. Probing classifiers: Promises, shortcomings, and advances. *Computational Linguistics*, 48(1):207–219, 2022.
- Nora Belrose, David Schneider-Joseph, Shauli Ravfogel, Ryan Cotterell, Edward Raff, and Stella Biderman. LEACE: Perfect linear concept erasure in closed form. In *Advances in Neural Information Processing Systems (NeurIPS)*, 2023.
- Yochai Blau and Tomer Michaeli. Rethinking lossy compression: The rate-distortion-perception tradeoff. In Kamalika Chaudhuri and Ruslan Salakhutdinov (eds.), *Proceedings of the 36th International Conference on Machine Learning (ICML)*, pp. 675–685, 2019.
- Zalán Borsos, Raphaël Marinier, Damien Vincent, Eugene Kharonov, Olivier Pietquin, Matthew Sharifi, Dominik Roblek, Olivier Teboul, David Grangier, Marco Tagliasacchi, and Neil Zeghidour. AudioLM: A language modeling approach to audio generation. In *IEEE/ACM Transactions on Audio, Speech, and Language Processing*, volume 31, pp. 2523–2533, 2023.
- Houwei Cao, David G. Cooper, Michael K. Keutmann, Ruben C. Gur, Ani Nenkova, and Ragini Verma. CREMA-D: Crowd-sourced emotional multimodal actors dataset. *IEEE Transactions on Affective Computing*, 5(4):377–390, 2014.
- Jingyi Chen, Zhimeng Guo, Jiyun Chun, Pichao Wang, Andrew Perrault, and Micha Elsner. Do audio LLMs really listen, or just transcribe? measuring lexical vs. acoustic emotion cues reliance. In *Proceedings of the 19th Conference of the European Chapter of the Association for Computational Linguistics (EACL)*, 2026.

-
- Yunfei Chu, Jin Xu, Qian Yang, Haojie Wei, Xipin Wei, Zhifang Guo, Yichong Leng, Yuanjun Lv, Jinzheng He, Junyang Lin, Chang Zhou, and Jingren Zhou. Qwen2-Audio: Technical report. *arXiv preprint arXiv:2407.10759*, 2024.
- Alexis Conneau, Germán Kruszewski, Guillaume Lample, Loïc Barrault, and Marco Baroni. What you can cram into a single token vector: Probing sentence embeddings for linguistic properties. In Iryna Gurevych and Yusuke Miyao (eds.), *Proceedings of the 56th Annual Meeting of the Association for Computational Linguistics (ACL)*, pp. 2126–2136, 2018.
- Santiago Cuervo, Skyler Seto, Maureen de Seyssel, Richard He Bai, Zijin Gu, Tatiana Likhomanenko, Navdeep Jaitly, and Zakaria Aldeneh. Closing the gap between text and speech understanding in LLMs. In *Proceedings of the 14th International Conference on Learning Representations (ICLR)*, 2026.
- Wenliang Dai, Junnan Li, Dongxu Li, Anthony Meng Huat Tiong, Junqi Zhao, Weisheng Wang, Boyang Li, Pascale Fung, and Steven C. H. Hoi. InstructBLIP: Towards general-purpose vision-language models with instruction tuning. In Alice Oh, Tristan Naumann, Amir Globerson, Kate Saenko, Moritz Hardt, and Sergey Levine (eds.), *Advances in Neural Information Processing Systems (NeurIPS 2023)*, volume 36, 2023.
- Alexandre Défossez, Laurent Mazaré, Manu Orsini, Amélie Royer, Patrick Pérez, Hervé Jégou, Edouard Grave, and Neil Zeghidour. Moshi: A speech-text foundation model for real-time dialogue. *arXiv preprint arXiv:2410.00037*, 2024.
- Monroe D. Donsker and S. R. Srinivasa Varadhan. Asymptotic evaluation of certain Markov process expectations for large time. IV. *Communications on Pure and Applied Mathematics*, 36(2):183–212, 1983.
- Fixie AI. Ultravox: An open, fast multimodal LLM. <https://github.com/fixie-ai/ultravox>, 2024.
- John Hewitt and Christopher D. Manning. A structural probe for finding syntax in word representations. In Jill Burstein, Christy Doran, and Thamar Solorio (eds.), *Proceedings of the 2019 Conference of the North American Chapter of the Association for Computational Linguistics: Human Language Technologies, NAACL-HLT*, pp. 4129–4138, 2019.
- Edward J. Hu, Yelong Shen, Phillip Wallis, Zeyuan Allen-Zhu, Yuanzhi Li, Shean Wang, Lu Wang, and Weizhu Chen. LoRA: Low-rank adaptation of large language models. In *Proceedings of the 10th International Conference on Learning Representations (ICLR)*, 2022.
- Minyoung Huh, Brian Cheung, Tongzhou Wang, and Phillip Isola. Position: The platonic representation hypothesis. In Ruslan Salakhutdinov, Zico Kolter, Katherine A. Heller, Adrian Weller, Nuria Oliver, Jonathan Scarlett, and Felix Berkenkamp (eds.), *Proceedings of the 41st International Conference on Machine Learning (ICML)*, volume 235, pp. 20617–20642, 2024.
- Anubhooti Jain, Mayank Vatsa, and Richa Singh. Words over pixels? rethinking vision in multimodal large language models. In *Proceedings of the 34th International Joint Conference on Artificial Intelligence (IJCAI), Survey Track*, pp. 10481–10489, 2025.
- Adrián Javaloy, Maryam Meghdadi, and Isabel Valera. Mitigating modality collapse in multimodal VAEs via impartial optimization. In Kamalika Chaudhuri, Stefanie Jegelka, Le Song, Csaba Szepesvári, Gang Niu, and Sivan Sabato (eds.), *International Conference on Machine Learning, ICML 2022, 17-23 July 2022, Baltimore, Maryland, USA*, volume 162 of *Proceedings of Machine Learning Research*, pp. 9938–9964. PMLR, 2022. URL <https://proceedings.mlr.press/v162/javaloy22a.html>.
- Leonid V. Kantorovich and G. Sh. Rubinstein. On a space of totally additive functions. *Vestnik Leningradskogo Universiteta*, 13(7):52–59, 1958.
- Siddharth Karamcheti, Suraj Nair, Ashwin Balakrishna, Percy Liang, Thomas Kollar, and Dorsa Sadigh. Prismatic VLMs: Investigating the design space of visually-conditioned language models. In Ruslan Salakhutdinov, Zico Kolter, Katherine A. Heller, Adrian

-
- Weller, Nuria Oliver, Jonathan Scarlett, and Felix Berkenkamp (eds.), *Proceedings of the 41st International Conference on Machine Learning (ICML)*, volume 235 of *Proceedings of Machine Learning Research*, pp. 23123–23144, 2024.
- Amos Lapidoth. Nearest neighbor decoding for additive non-Gaussian noise channels. *IEEE Transactions on Information Theory*, 42(5):1520–1529, 1996.
- Weixin Liang, Yuhui Zhang, Yongchan Kwon, Serena Yeung, and James Y. Zou. Mind the gap: Understanding the modality gap in multi-modal contrastive representation learning. In Sanmi Koyejo, S. Mohamed, A. Agarwal, Danielle Belgrave, K. Cho, and A. Oh (eds.), *Advances in Neural Information Processing Systems (NeurIPS)*, volume 35, 2022.
- Tsung-Yi Lin, Michael Maire, Serge J. Belongie, James Hays, Pietro Perona, Deva Ramanan, Piotr Dollár, and C. Lawrence Zitnick. Microsoft COCO: Common objects in context. In David J. Fleet, Tomás Pajdla, Bernt Schiele, and Tinne Tuytelaars (eds.), *Proceedings of the European Conference on Computer Vision (ECCV)*, pp. 740–755, 2014.
- Haotian Liu, Chunyuan Li, Qingyang Wu, and Yong Jae Lee. Visual instruction tuning. In Alice Oh, Tristan Naumann, Amir Globerson, Kate Saenko, Moritz Hardt, and Sergey Levine (eds.), *Advances in Neural Information Processing Systems (NeurIPS 2023)*, volume 36, 2023.
- Neri Merhav, Gideon Kaplan, Amos Lapidoth, and Shlomo Shamai. On information rates for mismatched decoders. *IEEE Transactions on Information Theory*, 40(6):1953–1967, 1994.
- Maxime Oquab, Timothée Darcet, Théo Moutakanni, Huy V. Vo, Marc Szafraniec, Vasil Khalidov, Pierre Fernandez, Daniel Haziza, Francisco Massa, Alaaeldin El-Nouby, Mido Assran, Nicolas Ballas, Wojciech Galuba, Russell Howes, Po-Yao Huang, Shang-Wen Li, Ishan Misra, Michael Rabbat, Vasu Sharma, Gabriel Synnaeve, Hu Xu, Hervé Jégou, Julien Mairal, Patrick Labatut, Armand Joulin, and Piotr Bojanowski. DINOv2: Learning robust visual features without supervision. *Transactions on Machine Learning Research*, 2024.
- Vassil Panayotov, Guoguo Chen, Daniel Povey, and Sanjeev Khudanpur. LibriSpeech: An ASR corpus based on public domain audio books. In *Proceedings of the IEEE International Conference on Acoustics, Speech and Signal Processing (ICASSP)*, pp. 5206–5210, 2015.
- Karol J. Piczak. ESC: Dataset for environmental sound classification. In Xiaofang Zhou, Alan F. Smeaton, Qi Tian, Dick C. A. Bulterman, Heng Tao Shen, Ketan Mayer-Patel, and Shuicheng Yan (eds.), *Proceedings of the 23rd ACM International Conference on Multimedia*, pp. 1015–1018, 2015.
- Alec Radford, Jong Wook Kim, Chris Hallacy, Aditya Ramesh, Gabriel Goh, Sandhini Agarwal, Girish Sastry, Amanda Askell, Pamela Mishkin, Jack Clark, Gretchen Krueger, and Ilya Sutskever. Learning transferable visual models from natural language supervision. In Marina Meila and Tong Zhang (eds.), *Proceedings of the 38th International Conference on Machine Learning (ICML)*, pp. 8748–8763, 2021.
- Alec Radford, Jong Wook Kim, Tao Xu, Greg Brockman, Christine McLeavey, and Ilya Sutskever. Robust speech recognition via large-scale weak supervision. In Andreas Krause, Emma Brunskill, Kyunghyun Cho, Barbara Engelhardt, Sivan Sabato, and Jonathan Scarlett (eds.), *Proceedings of the 40th International Conference on Machine Learning (ICML)*, volume 202 of *Proceedings of Machine Learning Research*, pp. 28492–28518, 2023.
- Jonathan Scarlett, Albert Guillén i Fàbregas, Anelia Somekh-Baruch, and Alfonso Martinez. Information-theoretic foundations of mismatched decoding. *Foundations and Trends in Communications and Information Theory*, 17(2–3):149–401, 2020.
- Tristan Thrush, Ryan Jiang, Max Bartolo, Amanpreet Singh, Adina Williams, Douwe Kiela, and Candace Ross. Winoground: Probing vision and language models for visio-linguistic compositionality. In *Proceedings of the IEEE/CVF Conference on Computer Vision and Pattern Recognition (CVPR)*, pp. 5238–5248, 2022.

Peter Tong, Ellis Brown, Penghao Wu, Sanghyun Woo, Adithya Iyer, Sai Charitha Akula, Shusheng Yang, Jihan Yang, Manoj Middepogu, Ziteng Wang, Xichen Pan, Rob Fergus, Yann LeCun, and Saining Xie. Cambrian-1: A fully open, vision-centric exploration of multimodal LLMs. *arXiv preprint arXiv:2406.16860*, 2024.

Cédric Villani. *Optimal Transport: Old and New*. Springer, 2009.

Mert Yükekşönül, Federico Bianchi, Pratyusha Kalluri, Dan Jurafsky, and James Zou. When and why vision-language models behave like bags-of-words, and what to do about it? In *Proceedings of the 11th International Conference on Learning Representations (ICLR)*, 2023.

Xiaohua Zhai, Basil Mustafa, Alexander Kolesnikov, and Lucas Beyer. Sigmoid loss for language image pre-training. In *Proceedings of the IEEE/CVF International Conference on Computer Vision (ICCV)*, pp. 11941–11952, 2023.

Deyao Zhu, Jun Chen, Xiaoqian Shen, Xiang Li, and Mohamed Elhoseiny. MiniGPT-4: Enhancing vision-language understanding with advanced large language models. In *Proceedings of the 12th International Conference on Learning Representations (ICLR)*, 2024.

A Theoretical framework: detailed treatment

This appendix contains the detailed formal development outlined in §4. Each result is preceded by an informal intuitive statement followed by a complete proof.

A.1 Generalized Mutual Information (GMI)

Overview. A representation Z might encode some knowledge about a target Y (e.g., the next token), but how much of this knowledge can a given decoder *use*? Standard mutual information $I(Z; Y)$ answers this for a decoder that is optimally matched to the representations it gets. A text-trained LLM is not optimally matched to non-text representations. It was matched to text representations, not speech representations, or image representations. The appropriate measure is the *Generalized Mutual Information* (GMI) (Merhav et al., 1994; Scarlett et al., 2020).

We reuse the notation from §3: $q(y|z, c)$ is the decoder’s next-token distribution (Eq. 1), Z is the representation consumed by the LLM, C is the text context, and Y is the target token. Let $\ell(c, z, y) := \log q(y|z, c)$ be the decoder’s log-score (the log-probability it assigns to token y given representation z and context c), clipped at a floor $\eta = 1/|\mathcal{V}|$ (where \mathcal{V} is the decoder’s output vocabulary) to ensure boundedness.

Intuition. The GMI tells us how well the decoder can distinguish the “correct” representation from random alternatives:

$$\text{GMI} = \mathbb{E} \left[\underbrace{\text{Score of the true match}}_{\text{how well the decoder scores the actual } Z} - \underbrace{\text{LogSumExp over all alternatives}}_{\text{how well random } Z' \text{ would score on average}} \right].$$

If the decoder consistently assigns a higher score to the true representation than to a uniformly sampled one, then the GMI is large. If the decoder cannot distinguish which Z generated which Y (assigning the same score to both), then the GMI is zero. This is similar to the Donsker-Varadhan variational representation of KL divergence (Donsker & Varadhan, 1983), but applied to the decoder’s scoring function instead of an arbitrary test function.

Formally, for a joint distribution P over (C, Z, Y) (which is either the text distribution P_T or the modal distribution P_M from §3), the GMI is given by:

$$\text{GMI}_P(q) = \mathbb{E}_{(C, Z, Y) \sim P} \left[\ell(C, Z, Y) - \log \mathbb{E}_{Z' \sim P(\cdot|C, Y)} \left[e^{\ell(C, Z', Y)} \right] \right]. \quad (3)$$

Theorem 1 (Accessible rate = GMI; following Scarlett et al., 2020). *Under i.i.d. sampling from P_M and standard measurability conditions, the maximum rate extractable by the fixed decoder q is $R_{\text{acc}}(P_M, q) = \text{GMI}_{P_M}(q)$.*

This is a classical result from the mismatched decoding literature; we state it here for completeness and to establish notation. The proof follows directly from the random-coding argument of Scarlett et al. (2020), Chapters 2–3, with constant-composition codebooks and the GMI decoder metric. The main idea is that the decoder q defines a fixed scoring rule (fixed at inference, regardless of how it was trained), and the maximum rate extractable under this rule, averaged over random codebooks distributed according to P_M , approaches $\text{GMI}_{P_M}(q)$.

A.2 GMI-Wasserstein bound

Next we bound the degradation of GMI when the decoder operates on the modal representations P_M rather than the text representations P_T it was trained on. The basic idea is as follows: if modal representations are sufficiently close to text representations, then the decoder should achieve near the same performance on them. How “sufficiently close” is determined by two properties of the decoder: how sensitive the decoder is to small perturbations of its inputs, and how large the space of representations is. Theorem 2 relies on three assumptions: the shared marginal (Assumption 1), the Lipschitz condition on the decoder (Assumption 2), and bounded support (Assumption 3).

Assumption 1 (Shared marginal). *The text and modal laws have the same prompts and target tokens: $P_M(C, Y) = P_T(C, Y)$.*

Assumption 2 (Local Lipschitz log-score). *There exists $L_{\log} > 0$ such that for all (c, y) and all z, z' in the typical-state region \mathcal{Z} : $|\ell(c, z, y) - \ell(c, z', y)| \leq L_{\log} \|z - z'\|$.*

That is, perturbing the representation by any amount changes the log-probability assigned by the decoder by at most L_{\log} times that amount. L_{\log} encodes the sensitivity of the decoder to changes to the input. Neural networks with smooth activations meet this condition locally; we measure L_{\log} empirically using gradient norms (§5.6).

Assumption 3 (Bounded typical-state region). *The typical-state region \mathcal{Z} has diameter $D = \sup_{z, z' \in \mathcal{Z}} \|z - z'\|$, which is finite and $O(\sqrt{d})$ after LayerNorm.*

This means the representations that are actually used in practice are confined to a bounded region, rather than being distributed throughout \mathbb{R}^d . This is precisely what LayerNorm accomplishes: all hidden states are projected onto a hypersphere of radius \sqrt{d} .

Theorem 2 (GMI-Wasserstein bound). *Under Assumptions 1, 2, and 3:*

$$|\text{GMI}_{P_M}(q) - \text{GMI}_{P_T}(q)| \leq (1 + e^{L_{\log} \cdot D}) \cdot L_{\log} \cdot \mathbb{E}_{(C, Y)} [W_1(P_M(Z|C, Y), P_T(Z|C, Y))]. \quad (4)$$

Intuition.

$$\underbrace{|\text{GMI}_{\text{text}} - \text{GMI}_{\text{modal}}|}_{\text{How much information is lost}} \leq \underbrace{(1 + e^{L_{\log} \cdot D})}_{\text{Penalty for distributional shape}} \cdot \underbrace{L_{\log}}_{\text{Decoder sensitivity}} \cdot \underbrace{\mathbb{E}[W_1(P_M, P_T)]}_{\text{Distributional distance}}$$

The difference between how much information the decoder can get from text representations and how much it can get from modal representations is that distance between distributions, multiplied by the strength of the decoder. But we have W_1 of the distributions, not the distance between the means; getting the mean of the modal distribution to the mean of the text distribution is not enough. If the modal distribution has a different shape, or spread, or tails, then the exponential penalty factor $(1 + e^{L_{\log} \cdot D})$ gets them. This is why the text-aligned encoders help to bound (they project on text-like directions, so they decrease both the distance and the shape mismatch), but mean centering would not.

The prefactor $(1 + e^{L_{\log} \cdot D})$ comes from the “competition term” in the proof (below). In the ambient space this prefactor is trivially large ($L_{\log} \cdot D$ ranges from 10 to 150) and the support-restricted bound (§A.3) refines it in terms of the effective support diameter.

A.2.1 Proof of Theorem 2

Proof overview. There are two terms in the GMI: (A) the expected score of the true representation, and (B) the expected score of a random representation. We must prove that the quantity in both (A) and (B) change very little when we replace the text representations with the modal representations. For (A), this is a corollary of the Lipschitz assumption. For (B), we have a potential complication of an exponential of the scores. However, the bounded-diameter assumption ensures that representations are all contained in a bounded region, which prevents large changes due to the exponential.

Setup. We denote $\ell(z) \equiv \ell(c, z, y)$ for fixed (c, y) . The GMI functional separates as $\Gamma(P) = A(P) - B(P)$ where:

$$A(P) = \mathbb{E}_{Z \sim P}[\ell(Z)] \quad (\text{direct term: expected score of the correct representation}) \quad (5)$$

$$B(P) = \log \mathbb{E}_{Z \sim P}[e^{\ell(Z)}] \quad (\text{competition term: how well random alternatives score}) \quad (6)$$

We derive upper bounds for $|A(P_M) - A(P_T)|$ and $|B(P_M) - B(P_T)|$ separately.

Step 1: Direct term (how much does the correct representation’s score change?). We would like to bound how much the expected score changes when we go from P_T to P_M . The Kantorovich–Rubinstein theorem (Kantorovich & Rubinstein, 1958; Villani, 2009) states that: if a function changes by at most L when you change its input by 1 unit (L -Lipschitz), then the difference in its expectation w.r.t. two distributions is at most L times the Wasserstein distance between the two distributions. Since ℓ is L_{\log} -Lipschitz (Assumption 2):

$$|A(P_M) - A(P_T)| = |\mathbb{E}_{P_M}[\ell] - \mathbb{E}_{P_T}[\ell]| \leq L_{\log} \cdot W_1(P_M, P_T). \quad (7)$$

If modal and text representations are similar (small W_1), and the decoder scores are smooth (small L_{\log}), then the expected score changes by a tiny amount.

Step 2: Competition term (how much does the random-alternative score change?). This is harder because $B(P) = \log \mathbb{E}[e^{\ell(Z)}]$ involves an exponential of the score, which means small differences are magnified. We can use a coupling π : a way of pairing up samples from P_M and P_T (think of arranging modal representations alongside the text representations they resemble the most). For each pair (Z_M, Z_T) , define $\Delta\ell = \ell(Z_M) - \ell(Z_T)$ as the difference in score between paired representations. By the Lipschitz assumption, $|\Delta\ell| \leq L_{\log} \cdot \|Z_M - Z_T\|$, and by the bounded diameter (Assumption 3), $|\Delta\ell| \leq L_{\log} \cdot D$.

Write $m(P) = \mathbb{E}_{Z \sim P}[e^{\ell(Z)}]$. Then:

$$\frac{m(P_M)}{m(P_T)} = \mathbb{E}_{\pi} \left[\frac{e^{\ell(Z_M)}}{m(P_T)} \right] = \mathbb{E}_{\pi} \left[\frac{e^{\ell(Z_T)}}{m(P_T)} \cdot e^{\Delta\ell} \right]. \quad (8)$$

The first term, $e^{\ell(Z_T)} / m(P_T)$, is a probability density under P_T (it sums to 1). The second term, $e^{\Delta\ell}$ accounts for the change in the score when moving from Z_T to Z_M . Since $|e^x - 1| \leq |x| \cdot e^{|x|}$ for bounded $|x| \leq L_{\log}D$:

$$\left| \frac{m(P_M)}{m(P_T)} - 1 \right| \leq e^{L_{\log}D} \cdot \mathbb{E}_{\pi}[|\Delta\ell|] \leq e^{L_{\log}D} \cdot L_{\log} \cdot \mathbb{E}_{\pi}[\|Z_M - Z_T\|]. \quad (9)$$

Using $|\log(1+x)| \leq |x|$ for $|x| < 1$ (applies when W_1 is small enough that the ratio stays near 1):

$$|B(P_M) - B(P_T)| = \left| \log \frac{m(P_M)}{m(P_T)} \right| \leq e^{L_{\log}D} \cdot L_{\log} \cdot W_1. \quad (10)$$

The $e^{L_{\log}D}$ term is the cost of the exponential: the competition term is more unstable to distributional shift than the direct term, because the former contains e^{ℓ} while the latter contains ℓ .

Step 3: Combine. The overall GMI change is at most the sum of the direct and competition terms:

$$|\Gamma(P_M) - \Gamma(P_T)| \leq \underbrace{L_{\log} \cdot W_1}_{\text{direct}} + \underbrace{e^{L_{\log} D} \cdot L_{\log} \cdot W_1}_{\text{competition}} = (1 + e^{L_{\log} D}) \cdot L_{\log} \cdot W_1. \quad (11)$$

The competition term dominates: it is $e^{L_{\log} D}$ times larger than the direct term. This is why the prefactor in the bound is so large and why the support-bounded corollary (which reduces D) is of practical value.

Step 4: Average over (C, Y) . Everything above was for a fixed prompt C and target Y . By Assumption 1 ($P_M(C, Y) = P_T(C, Y)$), the same prompts and targets appear under both laws, so we can simply average over all (C, Y) pairs to obtain the final bound.

When is the bound informative? The bound is a perturbation result: it is tightest when the mismatch W_1 is moderate relative to the decoder’s sensitivity. In the large-mismatch regime ($L_{\log} \cdot W_1 \gg 1$), the prefactor $(1 + e^{L_{\log} D})$ makes the right-hand side exceed the maximum possible GMI, and the bound becomes vacuous. In this regime, the bound correctly predicts that collapse occurs (the GMI ceiling is far below the matched-decoder rate) but cannot quantify how much information survives. Empirically, speech models operate in this regime ($L_{\log} \cdot W_1 = 19\text{--}162$), which is why the bound is loose for speech but informative for vision ($L_{\log} \cdot W_1 = 13\text{--}54$). The support-restricted corollary below partially addresses this by replacing the ambient diameter D with the smaller effective diameter D_{eff} , reducing the prefactor from $\sim e^{150}$ to $\sim e^7$.

A.3 Support-restricted bound

Support-restricted bound. If $P_M(Z|c, y)$ and $P_T(Z|c, y)$ are supported on some subset $\mathcal{S} \subseteq \mathcal{Z}$ such that $D_{\mathcal{S}} = \text{diam}(\mathcal{S}) \leq D$, then D may be replaced by $D_{\mathcal{S}}$ in Theorem 2.

Proof. If both marginals are supported in \mathcal{S} , any coupling π will also be supported on $\mathcal{S} \times \mathcal{S}$, so $\|Z_M - Z_T\| \leq D_{\mathcal{S}}$ for π -a.e. (Z_M, Z_T) . Step 2 above then gives that $|\Delta \ell| \leq L_{\log} \cdot D_{\mathcal{S}}$, which is the improved constant factor.

Why this matters. The ambient diameter D makes the prefactor $(1 + e^{L_{\log} D})$ extremely large ($L_{\log} \cdot D$ ranges from 10 to 150), while representations in modal and text space frequently lie in a far smaller effective volume. We estimate the effective support diameter D_{eff} from the participation ratio of the pooled representation covariance (§5.6), yielding $L_{\log} \cdot D_{\text{eff}} \in [3, 7]$ and a moderate prefactor ($\sim 20\text{--}1100$).

A.4 Per-type prediction

The theory predicts the overall trend: text-correlated information types (lexical) should strengthen or hold steady through the LLM, while non-text types (speaker, emotion, acoustic) should weaken. This qualitative prediction holds across all five models.

A stronger prediction would be that the degree of weakening for each information type matches its share of modality-specific variance. This does not hold at the level of individual types (Spearman $\rho = -0.40$, $p = 0.60$ across the four speech information types in Ultravox). The likely cause is the content-dependent L_{\log} : the Lipschitz constant varies $2.5\times$ across audio types ($L_{\log} = 14.58$ for speech vs. 5.92 for environmental sounds in Ultravox), acting as an additional driver of degradation independent of geometric alignment. A per-type bound would need to incorporate this content-dependence, replacing the scalar L_{\log} with a type-conditional $L_{\log}(\tau)$.

A.5 Probe-decoder asymmetry

Theorem 3 (Probe penalty). Let $h(a|z)$ be a linear probe with $\log h$ being L_h -Lipschitz in z . Then: $|\mathbb{E}_{P_M}[\log h(A|Z)] - \mathbb{E}_{P_T}[\log h(A|Z)]| \leq L_h \cdot W_1(P_M, P_T)$.

Proof. Identical to Step 1 of the Theorem 2 proof, replacing ℓ with $\log h$ and L_{\log} with L_h . Also there is no competition term for probes (no random-coding argument), so the exponential prefactor does not appear.

The key asymmetry. A linear probe is a simple model: one matrix multiplication followed by a softmax. Its sensitivity to distributional shift (L_h) is therefore simply the norm of the weights of that matrix. The LLM decoder is a deep transformer with billions of parameters, and its sensitivity (L_{\log}) reflects that depth. Empirically, $L_{\log}/L_h \approx 30\times$ (§5.6).

Now consider the same distributional shift with modal representations replacing text representations. The probe’s bound says degradation $\leq L_h \cdot W_1$ (small). The decoder’s bound says degradation $\leq (1 + e^{L_{\log}D}) \cdot L_{\log} \cdot W_1$ (large). Same shift, different impact. This is the formal basis for the “present but inaccessible” phenomenon: a probe can still read the information because it is a simple, low-sensitivity instrument, but the decoder’s complex scoring rule is far more sensitive to the distributional mismatch and cannot use it.

B Experimental details

B.1 Hook points and probing hyperparameters

Model	Encoder	Adapter	LLM-16	LLM-final
Ultravox	audio_tower. layer_norm	multi_modal_projector. ln_post	language_model. model.layers.16	language_model. model.norm
Qwen2-Audio	audio_tower. layer_norm	multi_modal_projector	language_model. model.layers.16	language_model. model.norm
LLaVA	...vision_tower. ...post.layernorm	model.mm.projector	...language_model. layers.16	...language_model. norm

Table 4: Hook points for representation extraction.

Logistic regression with ℓ_2 regularization ($C = 1.0$, scikit-learn default). Five random seeds (42, 43, 44, 45, 46). 80/20 stratified train/test split. Input features z-score normalized. Mean \pm std reported.

B.2 Lipschitz estimation

L_{\log} estimated via the 2-nearest-neighbor gradient norm method over $n = 1,000$ samples. For each sample z_i , we compute $\|\nabla_z \log q(y_i|z_i, c_i)\|$ via autograd. The 95th percentile of the resulting distribution serves as the L_{\log} estimate.

B.3 Extraction prompts

For the representation extraction experiments, we provide each model with a minimal, task-agnostic input to prevent the hidden states from being biased toward a specific downstream task. The representations are always extracted from the intermediate hook locations, not from the output.

Speech models. Ultravox receives the audio placeholder token `<|audio|>` wrapped in the model’s chat template (system/user/assistant turns). Qwen2-Audio requires a text prompt alongside audio; we use “Describe this audio.” in the user turn.

Vision models. LLaVA receives “<image>\nDescribe this image.” as the user message. Both Prismatic VLMs receive “Describe this image.” formatted via the Vicuna chat template.

Text baselines. Text baselines (Llama-3.1-8B for speech models, Vicuna-7B for vision models) process raw transcripts or captions with no additional prompt, using the model’s default tokenization.

B.4 LoRA experiment details

The emotion LoRA (§6.1) uses standard causal LM fine-tuning on Ultravox with a forced-choice emotion detection objective on CREMA-D.

LoRA configuration. Rank $r=16$, $\alpha=32$, dropout 0.05, target modules: q_proj, k_proj, v_proj, o_proj.

Training. AdamW optimizer, learning rate 10^{-4} , weight decay 0.01, gradient accumulation 8 steps (effective batch size 8), gradient clipping at max norm 1.0, mixed precision (bfloat16), gradient checkpointing enabled. Five epochs with early stopping (patience 2, monitoring validation loss). Best checkpoint at epoch 5 (val loss 0.0842, token accuracy 96.7%).

Prompt template. Each training sample uses a three-turn chat format:

- *System*: “You are an expert speech analyst. When presented with audio, identify the emotion expressed by the speaker. Always prioritize what you HEAR in the audio.”
- *User*:
Audio: <|audio|> \n\n QUESTION: What emotion is the speaker expressing? \n CHOICES: ["anger", "disgust", "fear", "happy", "neutral", "sadness"] \n\n Your answer MUST be exactly one of the CHOICES above, copied verbatim. \n Output JSON only: {"answer": "<exact choice>"}
- *Assistant*: {"answer": "<emotion>"} (training target)

We calculate the loss only on the assistant response tokens, while the input/prompt tokens are masked (with label -100).

Data split. CREMA-D (7,442 clips, 91 speakers, 6 emotions). 80/20 stratified split yields 1,002 held-out evaluation samples (167 per emotion class), saved deterministically for reproducibility.

Baseline evaluation. Base Ultravox (no LoRA) achieves 17.3% task accuracy on the held-out split (near chance for 6 classes), defaulting to “neutral” for most inputs.

B.5 Full probe accuracy tables

Table 5 reports the full probe accuracies (mean \pm std over 5 seeds) at all four hook points for every model–dataset–information-type combination. The main finding is that probe accuracy for non-text information types remains well above chance even at the LLM’s final layer, confirming that the information survives the decoder’s processing. It is the decoder’s *use* of this information, not its *presence*, that fails.

B.6 Information retention overview

Table 6 summarizes the information retention pattern across all five models. Retention is computed as the ratio of probe accuracy at the LLM’s final layer to probe accuracy at the adapter output, normalized by chance. Values above 100% indicate the LLM amplifies the signal; values below 100% indicate degradation. The pattern to notice is that non-text aligned encoders exhibit an asymmetric pattern (lexical content is amplified while speaker identity degrades), while text aligned encoders preserve or improve all the information types, simply because the encoder has already filtered out non-text information.

B.7 Detailed information retention

Table 7 provides the full breakdown of information retention per model and information type, with probe accuracies at the adapter and LLM-final layers.

Model	Info type (Dataset)	Encoder	Adapter	LLM-16	LLM-Final
Ultravox	Lexical (LS)	.422 ± .014	.279 ± .018	.570 ± .023	.535 ± .027
	Speaker (LS)	.721 ± .029	.605 ± .031	.628 ± .019	.556 ± .019
	Emotion (CD)	.679 ± .012	.621 ± .007	.603 ± .011	.557 ± .006
	Speaker (CD)	.508 ± .005	.196 ± .010	.204 ± .011	.137 ± .008
	Acoustic (E50)	.760 ± .033	.647 ± .041	.645 ± .035	.581 ± .032
Q2-Audio	Lexical (LS)	.270 ± .006	.242 ± .015	.506 ± .018	.471 ± .021
	Speaker (LS)	.980 ± .004	.961 ± .006	.665 ± .022	.589 ± .022
	Emotion (CD)	.866 ± .007	.874 ± .010	.880 ± .006	.877 ± .004
	Speaker (CD)	.880 ± .009	.816 ± .003	.725 ± .016	.556 ± .012
	Acoustic (E50)	.955 ± .005	.946 ± .011	.962 ± .004	.965 ± .003
LLaVA	Lexical (CO)	.629 ± .011	.620 ± .010	.675 ± .004	.669 ± .006
	Object cat. (CO)	.784 ± .011	.770 ± .009	.793 ± .010	.808 ± .011
	Super cat. (CO)	.802 ± .011	.797 ± .007	.833 ± .009	.842 ± .012
Prism.-D	Lexical (CO)	.608 ± .007	.637 ± .011	.652 ± .011	.664 ± .011
	Object cat. (CO)	.795 ± .016	.792 ± .015	.794 ± .014	.792 ± .012
	Super cat. (CO)	.837 ± .013	.832 ± .010	.834 ± .011	.839 ± .014
	Obj. count (CO)	.581 ± .017	.594 ± .015	.611 ± .015	.614 ± .016
	Obj. size (CO)	.667 ± .006	.679 ± .010	.693 ± .010	.688 ± .007
	Spatial spr. (CO)	.470 ± .013	.465 ± .025	.475 ± .010	.487 ± .008
Prism.-S	Lexical (CO)	.638 ± .007	.657 ± .008	.679 ± .007	.663 ± .009
	Object cat. (CO)	.813 ± .007	.804 ± .011	.811 ± .010	.819 ± .014
	Super cat. (CO)	.837 ± .013	.832 ± .017	.849 ± .010	.851 ± .010
	Obj. count (CO)	.594 ± .003	.598 ± .013	.652 ± .007	.647 ± .014
	Obj. size (CO)	.654 ± .019	.669 ± .014	.722 ± .018	.699 ± .020
	Spatial spr. (CO)	.478 ± .021	.459 ± .015	.507 ± .014	.481 ± .023

Table 5: Full probe accuracy (mean ± std over 5 seeds) for all models, datasets, hook points, and information types.

Table 6: Information retention (adapter → LLM-final, %). Values >100% indicate the LLM *amplifies* information; <100% indicates degradation. Text-aligned encoders retain all types; non-aligned encoders amplify lexical content while speaker identity collapses by up to 39%. LS = LibriSpeech, CD = CREMA-D, CO = COCO.

Model	Encoder	Lexical	Best non-text	Worst non-text
<i>Encoder not text-aligned</i>				
Ultravox	Whisper	192%	92% (speaker, LS)	70% (speaker, CD)
Qwen2-Audio	Whisper	195%	102% (acoustic)	61% (speaker, LS)
Prismatic-D	DINOv2	104%	101% (super cat.)	100% (object cat.)
<i>Encoder text-aligned</i>				
LLaVA	CLIP	108%	106% (super cat.)	105% (object cat.)
Prismatic-S	SigLIP	101%	102% (obj. & super cat.)	102% (obj. & super cat.)

B.8 Lipschitz constants and Wasserstein distances

Table 8 reports the empirical Lipschitz constants and Wasserstein distances used to evaluate the bound in §5.2.

B.9 Audio-token-only pooling

Our standard extraction mean-pools LLM-layer activations over all sequence positions (system prompt, audio tokens, assistant prompt). This could dilute the audio signal. Ultravox’s processor exposes the audio token boundaries (`audio_token_start_idx`, `audio_token_len`), letting us restrict pooling to audio positions only. We re-extracted LLM representations with audio-only pooling and re-ran probes to compare.

Model	Info type (Dataset)	Adapter	LLM-Final	Retention (%)
<i>Encoder not text-aligned</i>				
Ultravox	Lexical (LS)	.279	.535	192
	Speaker (LS)	.605	.556	92
	Emotion (CD)	.621	.557	90
	Speaker (CD)	.196	.137	70
	Acoustic (E50)	.647	.581	90
Q2-Audio	Lexical (LS)	.242	.471	195
	Speaker (LS)	.961	.589	61
	Emotion (CD)	.874	.877	100
	Speaker (CD)	.816	.556	68
	Acoustic (E50)	.946	.965	102
Prism.-D	Lexical (CO)	.637	.664	104
	Object cat. (CO)	.792	.792	100
	Super cat. (CO)	.832	.839	101
<i>Encoder text-aligned</i>				
LLaVA	Lexical (CO)	.620	.669	108
	Object cat. (CO)	.770	.808	105
	Super cat. (CO)	.797	.842	106
Prism.-S	Lexical (CO)	.657	.663	101
	Object cat. (CO)	.804	.819	102
	Super cat. (CO)	.832	.851	102

Table 7: Information retention from adapter to LLM-final layer (probe accuracy ratio \times 100). Retention $>100\%$ means the LLM amplifies the signal; $<100\%$ means degradation. Non-aligned encoders show selective amplification (lexical recovers, speaker degrades); text-aligned encoders retain or slightly improve all types. LS = LibriSpeech, CD = CREMA-D, E50 = ESC-50, CO = COCO.

Model	Dataset	L_{\log}	L_{\log} (p95)	D	W_1	$L_{\log} \cdot W_1$
<i>Speech</i>						
Ultravox	LibriSpeech	9.08	14.58	10.3	17.8	162
	CREMA-D	5.82	9.70	17.0	–	–
	ESC-50	3.66	5.92	20.7	–	–
Q2-Audio	LibriSpeech	0.49	0.67	122.2	38.9	19.1
	CREMA-D	0.59	0.75	229.9	–	–
	ESC-50	0.47	0.59	202.5	–	–
<i>Vision</i>						
LLaVA	COCO	0.29	0.36	28.5	46.3	13.4
Prism.-D	COCO	0.40	0.49	35.7	50.4	20.2
Prism.-S	COCO	1.12	1.44	16.2	47.9	53.7

Table 8: Lipschitz constants (L_{\log} , mean and p95 of gradient norm distribution), representation diameter (D), Wasserstein-1 distance (W_1 at LLM layer 16), and their product. L_{\log} is content-dependent: it decreases as audio moves away from text (LibriSpeech $>$ CREMA-D $>$ ESC-50). $L_{\log} \cdot W_1$ is largest for Ultravox (162, strongest degradation) and smallest for LLaVA (13.4, no degradation). Prismatic-S has $2.8\times$ higher L_{\log} than Prismatic-D, consistent with the LLM being more responsive to text-aligned representations.

Table 9 shows the result: audio-only pooling produces nearly identical probe accuracies across all datasets and information types, with all deltas within $\pm 2.1\%$ and most under 1%. Restricting to audio tokens does not help, and in several cases slightly hurts. This is consistent with the LLM mixing information across sequence positions during processing, so that the audio-derived signal is available at non-audio positions by layer 16.

Dataset	Label	All-token	Audio-only	Δ
<i>LLM hidden layer 16</i>				
LibriSpeech	Speaker	.637 \pm .026	.639 \pm .023	+0.002
LibriSpeech	Lexical	.591 \pm .009	.581 \pm .019	-.011
CREMA-D	Speaker	.210 \pm .006	.213 \pm .009	+0.003
CREMA-D	Lexical	.999 \pm .001	.999 \pm .001	+0.000
CREMA-D	Emotion	.593 \pm .004	.595 \pm .006	+0.002
ESC-50	Sound	.681 \pm .027	.677 \pm .031	-.003
<i>LLM final layer</i>				
LibriSpeech	Speaker	.565 \pm .012	.544 \pm .020	-.021
LibriSpeech	Lexical	.573 \pm .024	.559 \pm .023	-.014
CREMA-D	Speaker	.140 \pm .009	.140 \pm .008	-.000
CREMA-D	Lexical	.999 \pm .001	.999 \pm .001	-.000
CREMA-D	Emotion	.556 \pm .008	.553 \pm .004	-.004
ESC-50	Sound	.613 \pm .016	.603 \pm .020	-.011

Table 9: Probe accuracy with all-token vs. audio-only pooling at LLM layers (Ultravox). All deltas are within $\pm 2.1\%$, most under 1%. Audio-only pooling does not improve probe accuracy.

The Prismatic comparison (Table 10) isolates encoder text-alignment as the causal variable. Both VLMs share the same architecture, adapter, training recipe, and LLM backbone; only the vision encoder differs. SigLIP (text-aligned) shows consistent improvement through the LLM for all information types, while DINOv2 (not text-aligned) shows stagnation or minimal change for non-textual attributes.

Encoder	Info type	Probe accuracy		
		Adapter	LLM-final	Δ_{LLM}
<i>Text-describable attributes</i>				
DINOv2	Lexical	.637	.664	+4.2%
	Object cat.	.792	.792	-0.0%
	Super cat.	.832	.839	+0.8%
SigLIP	Lexical	.657	.663	+0.9%
	Object cat.	.804	.819	+1.9%
	Super cat.	.832	.851	+2.3%
<i>Non-textual attributes</i>				
DINOv2	Obj. count	.594	.614	+3.4%
	Obj. size	.679	.688	+1.3%
	Spatial spr.	.465	.487	+4.7%
SigLIP	Obj. count	.598	.647	+8.2%
	Obj. size	.669	.699	+4.5%
	Spatial spr.	.459	.481	+4.8%

Table 10: Prismatic controlled comparison (full results). Δ_{LLM} = change from adapter to LLM-final. Top: text-describable attributes (named in captions). Bottom: non-textual attributes (object count, average object size, spatial spread; derived from annotations, not captions). Text baseline accuracy is substantially lower (.415–.495) for non-textual attributes, confirming their visual nature. Same architecture, same LLM, only encoder differs.

The mode alignment spectrum (Table 11) reveals which directions carry the mismatch. For each model, we decompose the adapter output covariance into eigenmodes and measure their text alignment. The dominant eigenmode is modality-specific ($\rho_k \ll 1$) for all non-text-aligned encoders, while for SigLIP even the dominant mode is text-aligned ($\rho_k = 0.83$).

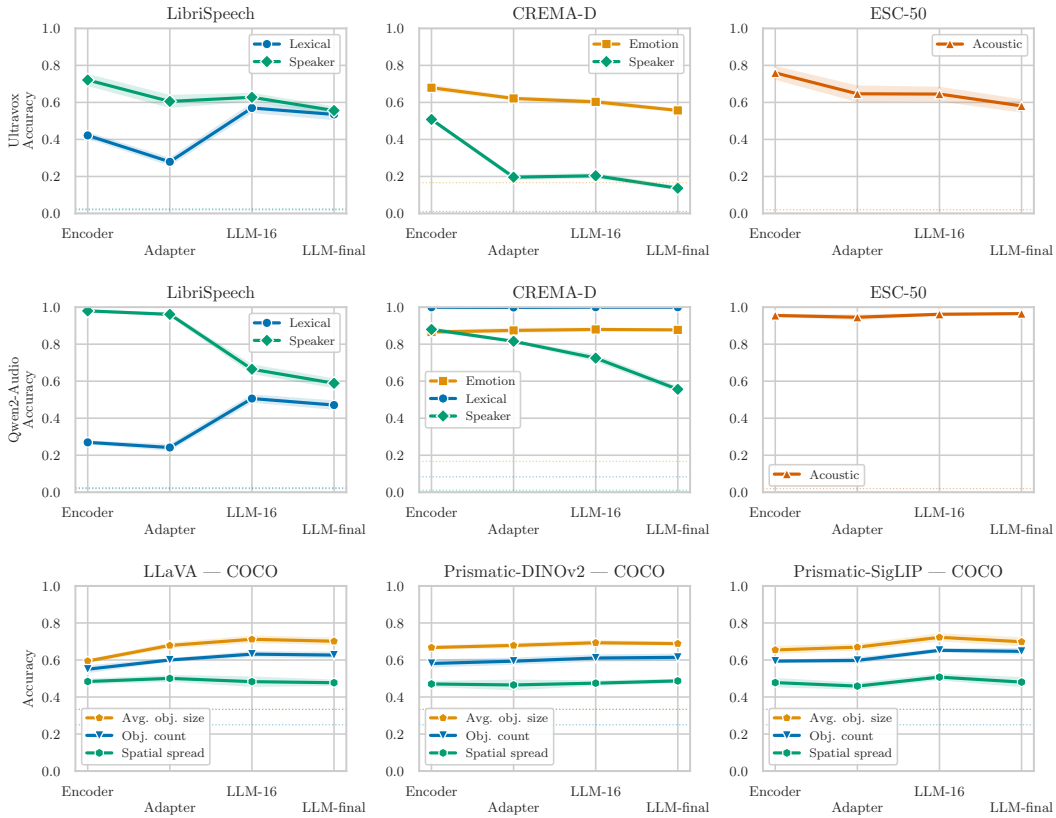


Figure 1: Linear probe accuracy at four extraction points (encoder, adapter, LLM layer 16, LLM final) for all five models. For speech models (rows 1–2), lexical accuracy increases through the LLM while speaker identity degrades, illustrating the information accessibility gap. For vision models (row 3), LLaVA and Prismatic-S (text-aligned encoders) show improvement across all information types, while Prismatic-D (non-aligned) shows flat or declining non-textual accuracy. Datasets: LibriSpeech, CREMA-D, ESC-50 (speech); COCO (vision).

Model	Mode 0 ρ_k	Mean ρ_k (top 10)	MS modes	MS var.
Ultravox	0.001	1.76	11/100	63.6%
Qwen2-Audio	0.010	7.21	5/100	97.6%
LLaVA	0.013	3.94	9/100	71.9%
Prismatic-D	0.034	0.087	53/100	71.0%
Prismatic-S	0.827	1.95	14/100	24.6%

Table 11: Mode alignment summary. MS modes = modes with $\rho_k < 0.5$ (modality-specific). MS var. = fraction of top-100 eigenmode variance in MS modes. Mode 0 is modality-specific ($\rho_k \ll 1$) for all non-text-aligned encoders; for SigLIP (text-aligned), even Mode 0 is text-aligned ($\rho_k = 0.83$). Extending to all 4096 modes strengthens the pattern: tail modes are overwhelmingly text-aligned with negligible individual variance, so the MS/TA split is driven by the high-variance modes reported here.

C Additional limitations

Scope. We test speech and vision across five models. The framework applies to any multimodal LLM with a text-trained decoder, but video/3D remain untested.

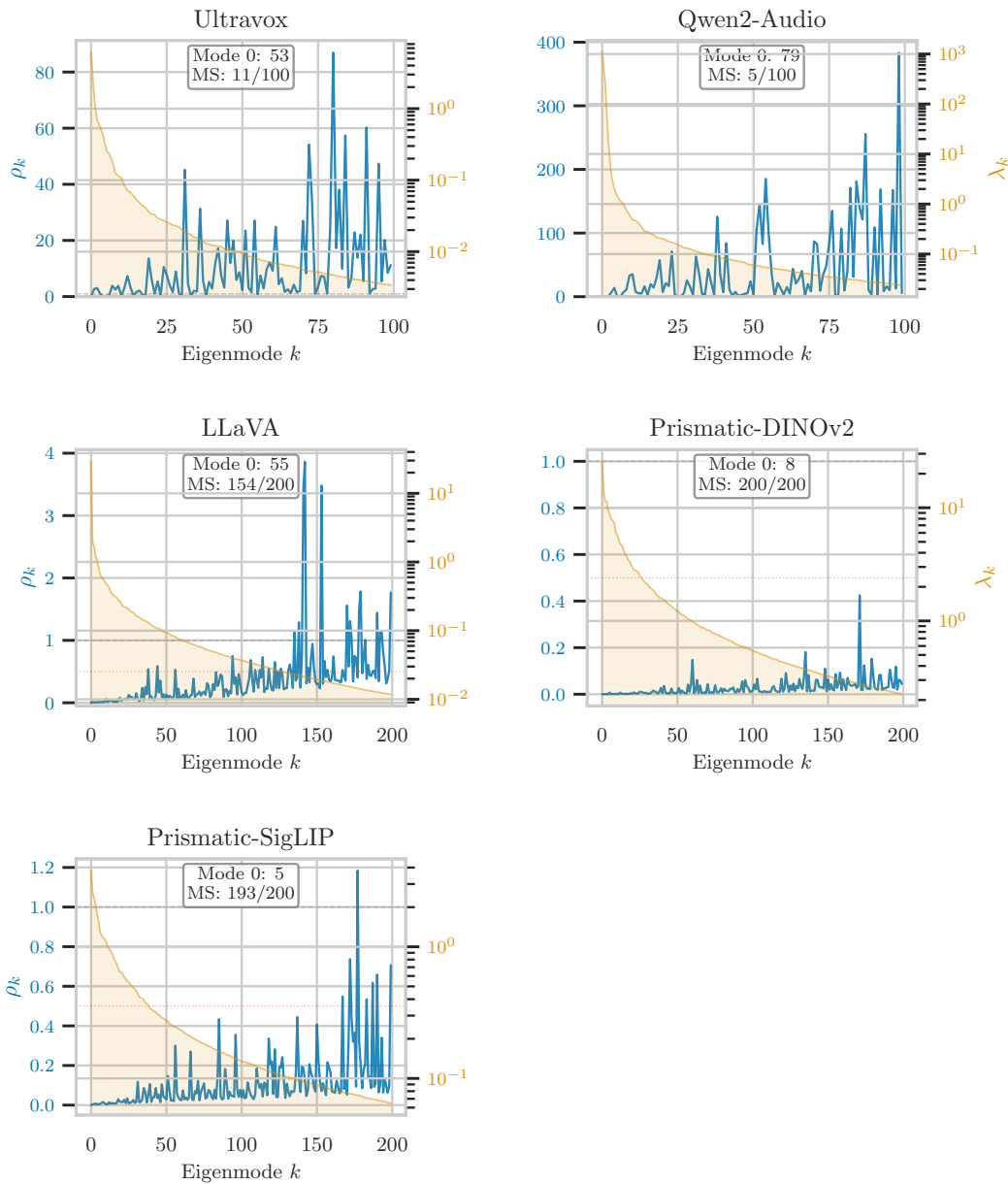


Figure 2: Mode alignment profiles for all five models. Each panel shows the top modes (eigenvectors of the adapter-output covariance Σ_M , sorted by decreasing eigenvalue; 100 for speech models, 200 for vision). Blue (left axis): alignment score ρ_k , the ratio of text variance to modal variance along each mode (§5.3). Orange (right axis): eigenvalue λ_k (log scale), the amount of adapter variance carried by each mode. Annotations show the percentage of total variance in Mode 0 and the count of modality-specific modes ($\rho_k < 0.5$). For non-aligned encoders, the highest-variance modes have $\rho_k \approx 0$: the adapter’s dominant variation is along directions the decoder has never seen. For Prismatic-S (SigLIP, text-aligned), even Mode 0 is text-aligned ($\rho_0 = 0.83$).

Assumption 1 (shared marginal). We assume $P_M(C, Y) = P_T(C, Y)$. This holds when the multimodal model is trained on text-centric tasks (transcription, captioning). Violations add a marginal-shift term independent of representation geometry.

Generality of the GMI constraint. The mechanistic explanation is not architectural: the text-shaped scoring rule of the multimodal LLM decoder is conditioned only on the text-

dominating training objective, and holds regardless of the adapter implementation (linear projection, MLP, Q-Former, perceiver resampler, discrete codebook, etc.). The GMI constraint is more broadly relevant for multimodal modelling: in the absence of a training objective that explicitly seeks out each modality, the decoder will remain indifferent to non-text directions.